G108 Journal of The Electrochemical Society, **153** (2) G108-G118 (2006)
0013-4651/2005/153(2)/G108/11/$15.00 © The Electrochemical Society

Irradiation-Induced Deep Levels in Silicon for Power Device Tailoring

R. Siemieniec,[a] F.-J. Niedernostheide,[b] H.-J. Schulze,[b] W. Südkamp,[c] U. Kellner-Werdehausen,[d] and J. Lutz[e]

[a]*Infineon Technologies Austria AG, A-9500 Villach, Austria*
[b]*Infineon Technologies AG, D-81726 Munich, Germany*
[c]*Aktiv Sensor GmbH Stahnsdorf, D-14532 Stahnsdorf, Germany*
[d]*Infineon Technologies AG, 59581 Warstein, Germany*
[e]*Chemnitz University of Technology, D-09107 Chemnitz, Germany*

This paper gives an overview of the physics and electrical characteristics of irradiation-induced defects in silicon created by electrons, protons, and helium ions. The parameters of the traps usable as recombination centers or causing doping and discharging effects are described quantitatively, including temperature dependence and injection level dependence. The influence of recombination centers on the electric characteristics of power devices is discussed, especially with respect to applications for medium-voltage and high-voltage power devices.
 [DOI: 10.1149/1.2137649]

Manuscript submitted April 25, 2005; revised manuscript received September 2, 2005.
Available electronically December 14, 2005.

Irradiation techniques for carrier lifetime control are commonly used for optimizing power devices such as free-wheeling diodes (FWDs), gate-turn-off (GTO) thyristors, or insulated gate bipolar transistors (IGBTs). Comparing the carrier lifetime adjustment by irradiation with the adjustment by impurities such as gold and platinum, irradiation techniques offer the possibility to reduce the carrier lifetime at the end of the fabrication process of the power devices and to create spatially varying lifetime profiles.

In high-power switching devices such as IGBTs and GTO thyristors, irradiation with light ions is used for a local reduction of the carrier lifetime to improve the turn-off behavior while still maintaining low on-state losses.[1,2] For creating fast-switching FWDs, the combination of electron and light-ion irradiation as well as light-ion irradiation with two different energies creating two areas with reduced carrier lifetime has been shown to be beneficial for soft reverse recovery behavior.[3,4]

Apart from controlling the local carrier lifetime, light-ion radiation can also be applied to modify the doping profile of silicon devices. This is especially important for power devices, which usually have a very high resistivity of the starting material to provide high blocking voltages. Proton-irradiated and subsequently annealed silicon shows the formation of shallow donors that are related to hydrogen-defect complexes.[5] Possible applications are the integration of an overvoltage protection function into thyristors[6] or the implementation of a field-stop layer in high-voltage devices. It is even possible to use both effects, local reduction of carrier lifetime and increasing the doping concentration, simultaneously by applying a single proton irradiation, as has been shown for local lifetime-controlled IGBTs with a punch-through (PT) structure.[7]

Recently,[8] hydrogen-induced donor formation has also been successfully applied to create CoolMOS transistors in which the compensation principle is used to increase the breakdown voltage of a MOS transistor while keeping the on-resistance very low. In this case, relatively high proton doses ($>10^{14}$ cm^{-2}) and annealing temperatures (>400°C) have been utilized.

Similar to conventional MOS structures, the CoolMOS transistor also has an internal diode. The switching behavior and the reverse recovery charge of this diode can be improved efficiently by moderate doses ($<5 \times 10^{12}$ cm^{-2}) of proton irradiation.[9] In this case, local lifetime reduction is the dominant effect, while hydrogen-induced donor formation is of minor importance. A similar improvement of the reverse recovery behavior of the internal CoolMOS diode can be achieved by electron irradiation.

Electron irradiation can also be used to enhance the performance of IGBTs with reverse blocking capability.[10,11] These devices suffer from a high reverse leakage current caused by the current gain of the inherent parasitic p-n$^-$-p$^+$ transistor, which is formed by the p-body, the n$^-$ substrate, and the p$^+$ emitter of the IGBT. An acceptable reduction of the carrier lifetime results in a lower current gain of the transistor without a significant increase in the forward losses and, therefore, in a remarkable decrease in the reverse leakage current. In a similar way, the current gain of the anode-side transistor in thyristors can be reduced locally to improve the breakdown voltage of thyristors. This has been shown for GTO thyristors[12] and light-triggered thyristors,[13] where a reduction of the current gain near the device edges, achieved by a masked electron irradiation, results in a significantly higher breakdown voltage.

Recombination Centers and Lifetime

The carrier lifetime obtained from deep-level recombination can be obtained by using the Shockley-Read-Hall (SRH) statistics.[14] Assuming equal excess carrier concentration for electrons, δn, and holes, δp, the SRH lifetime for an independent deep level is given by

$$\frac{1}{\tau_{SRH}} = \frac{n_0 + p_0 + \delta n}{\tau_{p0}(n_0 + n_1 + \delta n) + \tau_{n0}(p_0 + p_1 + \delta n)} \quad [1]$$

where τ_{n0} and τ_{p0} denote the minority carrier lifetimes of electrons and holes, n_0 and p_0 are the electron and hole equilibrium carrier concentrations, while the terms n_1 and p_1 are the equilibrium carrier concentrations corresponding to the Fermi-level position coincident with the recombination level position in the bandgap

$$n_1 = n_i \exp\left(\frac{E_T - E_I}{k_B T}\right) \quad [2]$$

$$p_1 = n_i \exp\left(\frac{E_I - E_T}{k_B T}\right) \quad [3]$$

In case of low-level injection $\delta n \ll n_0$ and in n-type silicon $n_0 \gg p_0$, Eq. 1 simplifies to Eq. 4, which shows that for recombination centers close to the middle of the bandgap, the low-level lifetime τ_{LL} is equal to the hole minority carrier lifetime τ_{p0}. Furthermore, low-level lifetime is controlled by traps close to the intrinsic level

$$\frac{1}{\tau_{LL}} = \frac{n_0}{\tau_{p0}(n_0 + n_1) + \tau_{n0}p_1} \quad [4]$$

During high-level injection, the excess carrier density is much higher than the equilibrium densities: $\delta n \gg n_0, n_1, p_0, p_1$. The high-level lifetime τ_{HL} is given by

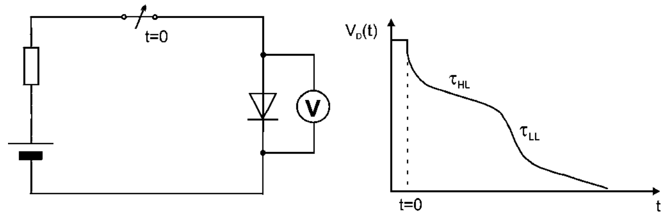

Figure 1. (a) OCVD principle; (b) OCVD voltage waveform.

$$\tau_{HL} = \tau_{n0} + \tau_{p0} = \frac{1}{c_n N_T} + \frac{1}{c_p N_T} \quad [5]$$

where c_n and c_p are the capture rates for electrons and holes, and N_T is the trap concentration.

The energy level of the recombination center has a strong influence on the low-level carrier lifetime, while the high-level lifetime does not directly depend on the energy level of the recombination center. High-level injection is found only if $\delta n \gg n_1,p_1$. If the condition $\delta n \gg n_1,p_1$ is not fulfilled, any measured high-level injection lifetime will apparently depend on excess carrier density.

If the density of free carriers is very low and there are no excess carriers, thus $n,p \ll n_i,n_1,p_1$, Eq. 1 simplifies to

$$\tau_{SC} = \tau_{p0} \exp\left(\frac{E_T - E_I}{k_B T}\right) + \tau_{n0} \exp\left(\frac{E_I - E_T}{k_B T}\right) \quad [6]$$

The generation lifetime τ_{SC} strongly depends on the energy level of the recombination center and has its maximum value if the energy level is equal to the intrinsic energy level.

Characterization Methods

In order to determine the characteristics of recombination centers, we used deep level transient spectroscopy (DLTS),[15] open circuit voltage decay (OCVD) measurements,[16] and spreading resistance (SR) measurements.[17] In the following section, some particularities concerning our OCVD and the SR measurements are briefly described.

OCVD measurements.— Using OCVD measurements, a steady-state excess carrier concentration is established by a forward current flow through a diode (Fig. 1a). After an abrupt opening of the circuit at $t = 0$, recombination of excess carriers will take place and the diode's open voltage V_D is monitored (Fig. 1b). The initial voltage step at $t = 0$ is due to the voltage drop V_0 in the diode, which is observed when the current flow stops. The strong drop in the time series of $V_D(t)$ near $t = 0$ is caused by emitter recombination. This effect becomes negligible for $t > 2.5\tau_b$, where τ_b is the base lifetime.[18] It is possible to estimate the high-injection lifetime as well as the low-injection lifetime from linear fits of different parts of the time series $V_D(t)$.

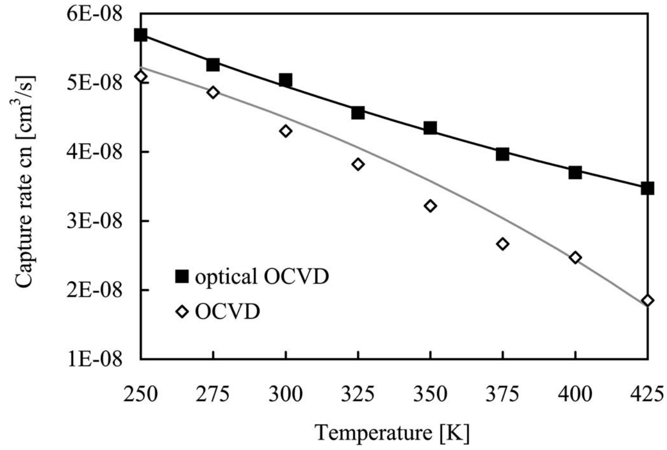

Figure 2. Measured electron capture rate of the OV center.

Applying OCVD measurements to diodes with a p-i-n structure, the lifetime under high-injection conditions (high-level lifetime) is given by Eq. 7

$$\tau_{HL} = \frac{2k_B T}{q}\left(\frac{dV}{dt}\right)^{-1} \quad [7]$$

The low-level lifetime is given by Eq. 8[19]

$$\tau_{LL} = \frac{k_B T}{q}\left(\frac{dV}{dt}\right)^{-1} \quad [8]$$

In the case of low-level lifetime measurements, parasitic elements such as capacities and shunt resistances of the measurement setup should be minimized because of their influence on the measurement results due to the low carrier concentrations. The validity of the measurement result depends on the charge stored inside the device in comparison with the value of external parasitics. If necessary, compensation techniques as described in Ref. 20 should be used. The excess carrier concentration in the low-doped base region may be approximated by use of Eq. 9

$$\bar{p} = n_i \exp\left(\frac{V_0}{\frac{2k_B T}{q}}\right) \quad [9]$$

If the energy level of the recombination center is relatively close to the conduction-band edge, optical generation of free carriers may become necessary in order to create the high excess carrier generation required for the OCVD technique. For these measurements, the primary wavelength of 1064 nm of a pulsed yttrium-aluminum-garnet (YAG) laser is used to generate excess carriers. At this wavelength, the absorption coefficient is approximately 10 cm^{-1}.[21,22] For such measurements, we used the diode-pumped, Q-switched YAG

Table I. Overview of irradiation-induced defects in silicon relevant for applications in power devices (found after annealing with temperatures >300°C). Shallow thermal and hydrogen-induced donors are also included.

Type	Physical nature	DLTS signal	Energy level
OV	Oxygen-vacancy complex	$E(90\ K)$	$E_C - 0.169$ eV
VV	Divacancy complex		
	−/2−	$E(130\ K)$	$E_C - 0.24$ eV
	0/−	$E(230\ K)$	$E_C - 0.43$ eV
V_4/V_5	Multivacancy complex	$E(230\ K)$	$E_C - 0.43$ eV
V_2O	Divacancy-oxygen complex	$E(230\ K)$	$E_C - 0.43$ eV
COVV	Carbon-oxygen complex	$H(195\ K)$	$E_V + 0.35$ eV
STD(H)	Hydrogen-related shallow thermal donors	—	E_C − (34-53 meV)
TDD	Thermal double-donor family	—	E_C − (61-135 meV)

Table II. Properties of the OV-center $E(90\ \mathrm{K})$.[42,43]

Energy (eV)	Capture rates (cm^3/s) Electrons	Capture rates (cm^3/s) Holes	Entropy factor Electrons	Entropy factor Holes
$E_C - 0.169$	$1.1505 \times 10^{-7} \exp\left(-\frac{T}{355.4\ \mathrm{K}}\right)$	$6.39 \times 10^{-7}\sqrt{\frac{T}{300\ \mathrm{K}}} \times \exp\left(\frac{6.15 \times 10^{-3}\ \mathrm{eV\ K}}{k_B T}\right)$	0.54	1.85

Laser JOL-R60 manufactured by JENOPTIK Germany.[23] The laser pulse width was about 100 ns with a pulse energy of 6 mJ. The pulse frequency was 3 kHz while the duration of one pulse sequence was about 1 ms. To ensure homogeneous excitation over the whole device area, the laser beam was defocused.

SR measurements.— Due to compensation effect as the result of charged deep levels, SR measurements can be used for the determination of the vertical distribution of recombination centers. The advantages of this method are its simplicity and robustness, and its applicability over large depths. The drawback is that, in the case of several energy levels, it is impossible to separate contributions from a specific trap. Furthermore, it is difficult to draw conclusions about the trap densities. In addition, the method is limited to resistivity changes that are in the same order of magnitude as the background doping.

Application-Relevant Deep Levels after Annealing

Irradiation-induced defects and their annealing behavior were investigated long before they were applied for carrier lifetime control.[24,25] While the properties of irradiation-induced defects created by electron irradiation,[5,24,26-32] proton irradiation,[5,25,33-40] and helium irradiation[5,35,41] in n-type silicon were intensively investigated, there are only a few publications dealing with irradiatedp-type silicon.[25,26,31,33,37,40] Table I gives an overview of irradiation-induced defects that have significant effects on the electrical behavior of power devices. Shallow thermal double donors (TDDs) and hydrogen-related shallow thermal donors STD(H) are also included because they may modify the electrical characteristics in power devices, in particular at higher annealing temperature ($>300°C$).

Center Characteristics and Applications

Carrier lifetime adjustment by the OV center.— Center properties.— A very important trap for electron-hole recombination in silicon power devices is the OV center or A center $E(90\ \mathrm{K})$. This acceptor-like defect is a vacancy-oxygen complex and is found after irradiation with electrons, protons, or helium ions. The OV center starts to anneal out at temperatures above 350°C and has almost completely vanished at an annealing temperature of 400°C.[5]

Its energy level is far from the middle of the bandgap, thus the defect does not decrease the low-level lifetime or increase the leakage current significantly, but acts as an effective recombination center under high-level injection conditions. In bipolar power devices such as FWDs, GTO thyristors, IGBTs, etc., the high-injection lifetime τ_{HL} controls forward characteristics as well as switching properties.

The data for the OV center listed in Table II were determined by DLTS measurements. As shown recently,[27] the temperature dependence of the capture rates cannot be extrapolated from the DLTS measurements over a wide temperature range, but has to be determined by other methods. Because the electron capture rate of the OV center is much lower than the hole-capture rate, it is possible to simplify Eq. 5 by eliminating the second term. Taking into account the recombination properties of the nonirradiated sample, we obtain

$$\frac{1}{\tau_{HL}} = c_n N_T + \frac{1}{\tau_0} \qquad [10]$$

where τ_0 is the high-injection lifetime of the nonirradiated silicon. The plot of the inverse high-injection lifetime τ_{HL} vs trap concentration N_T for various temperatures makes it possible to determine the temperature dependence of the electron capture rate.[42]

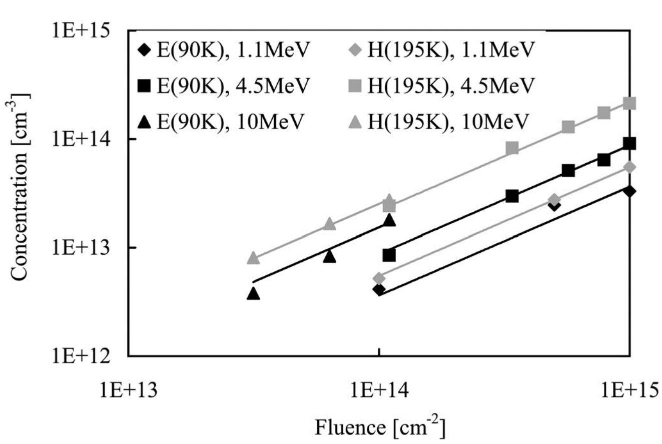

Figure 3. Concentration of the OV center $E(90\ \mathrm{K})$ and the K center $H(195\ \mathrm{K})$ with respect to the electron irradiation dose for an annealing temperature $>330°C$.

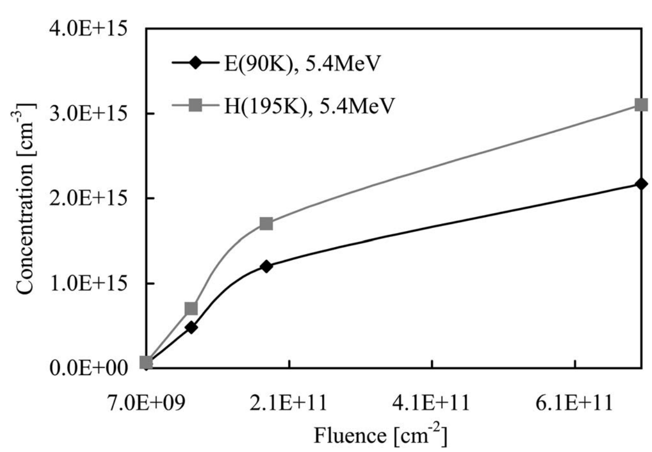

Figure 4. Peak density of the OV center $E(90\ \mathrm{K})$ and the K center $H(195\ \mathrm{K})$ with respect to the helium irradiation dose for an annealing temperature $>330°C$.

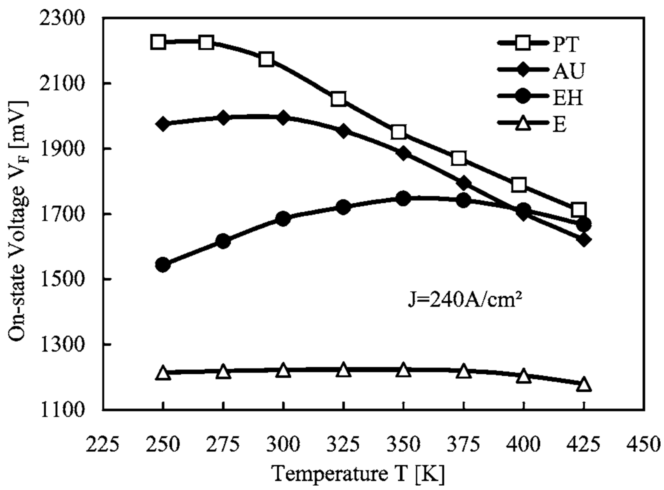

Figure 5. On-state voltage at a specified diode current as a function of the temperature for different carrier lifetime control techniques.

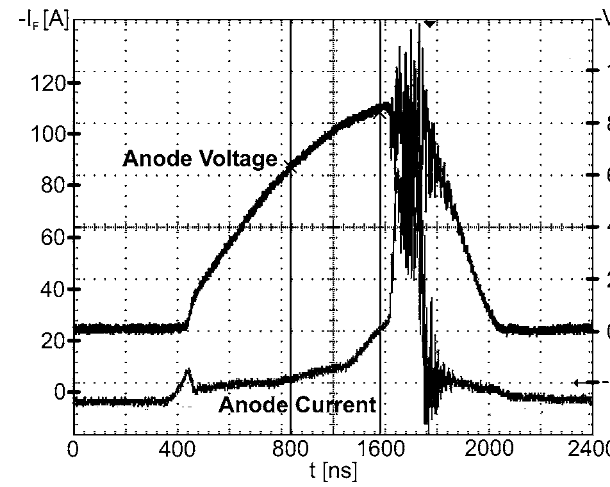

Figure 7. Measured current and voltage time series of an electron-irradiated 1.2-kV FWD with p^+-n^--n^+ structure during the turn-off period, showing dynamic IMPATT oscillation ($V_R = 910$ V, $I_F = 8$ A, $di/dt = 250$ A/μs, $T = 290$ K).

In the case of relatively shallow defects such as the OV center, very high excess carrier concentrations are necessary to create high-injection conditions in order to apply Eq. 5 and 10 for determination of the capture rate.[42] Optical generation of free carriers by means of a laser beam results in an excess carrier concentration of about 2×10^{17} to 4×10^{17} cm^{-3}. In Fig. 2, the capture rate determined in this way[43] is shown together with results of OCVD measurements based on electrical excitation with an excess carrier concentration of 2×10^{16} cm^{-3}. Another way to determine $c_n(T)$ is to exploit temperature-dependent microwave photoconductive measurements.[44] When $c_n(T)$ as determined by optical OCVD measurements with very high excess-carrier concentrations is used in device simulation, a good agreement between measured and simulated device properties is achieved.[42]

Defect concentration in dependence of irradiation parameters.— The knowledge of the resulting defect concentration after device irradiation is essential for predicting the device properties. In the case of electron irradiation, the defect concentration can be assumed to increase linearly with the electron dose over a broad range. Figure 3 shows the OV-center density in dependence of the flux for different electron energies after annealing at a temperature of $T > 330$°C, confirming the linear dependence.

In the case of proton or helium irradiation, large defect concentrations are generated in the area close to the end of range even for moderate doses. In Fig. 4, the peak value of the OV concentration profile is plotted as a function of the helium fluence after irradiation with an energy $E = 5.4$ MeV and annealing at a temperature of $T > 330$°C. The results suggest saturation behavior due to the limited concentration of oxygen and carbon atoms.

Adjustment of carrier lifetime.— The OV center is mainly responsible for changes in the high-injection carrier lifetime, which is essential for the optimization of bipolar power devices.

First, local or homogeneous reduction of the carrier lifetime reduces switching losses due to increased recombination of stored excess carriers. Combining local and homogeneous carrier lifetime reduction, even a change of the temperature dependence of important device parameters is possible. For example, Fig. 5 shows the temperature dependence of the on-state voltage drop at constant current of FWDs treated with different carrier lifetime control techniques. While the platinum- (Pt) and gold-diffused (Au) devices show a negative temperature coefficient, the electron-irradiated device (E) shows only a weak temperature dependence. The helium- and additionally electron-irradiated device (EH) has a positive temperature coefficient over a wide temperature range.[45] This property becomes important if several devices are connected in parallel to achieve higher current capability.

Another example is the improvement of the switching behavior of FWDs (Fig. 6). In this example, it is important for the device to have a soft reverse-recovery behavior in order to avoid—or at least to minimize—overvoltages caused by parasitic inductive elements. Otherwise, a snap-off of the reverse current will result in a very high di/dt, which will cause large overvoltages even in the case of a small inductance. One efficient way to ensure soft reverse-recovery behavior is to combine local and homogeneous carrier lifetime reduction so that the recombination center peak is close to the p-n junction.[3]

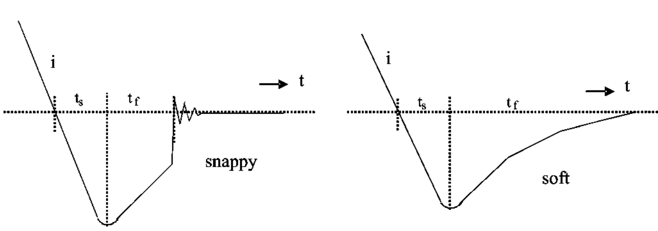

Figure 6. Example of the switching behavior of free-wheeling diodes.

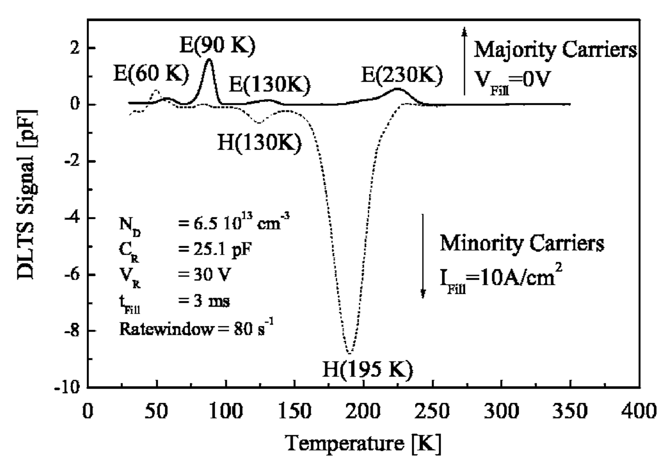

Figure 8. Minority and majority DLTS spectra measured in the n^--layer of a p^+-n^--n^+ diode after helium irradiation and subsequent annealing at 350°C.

Table III. Properties of the K-center $H(195\ \mathrm{K})$.[42]

Energy (eV)	Capture rates ($\mathrm{cm^3/s}$)		Entropy factor	
	Electrons	Holes	Electrons	Holes
$E_V + 0.353$	$9.85 \times 10^{-9}\sqrt{\frac{T}{300\ \mathrm{K}}}\exp\left(-\frac{85 \times 10^{-3}\ \mathrm{eV\ K}}{k_B T}\right)$	$4.3 \times 10^{-9}\sqrt{\frac{T}{300\ \mathrm{K}}}$	0.25	3.96

Temporary doping effects related to the COVV complex.— Center properties.— The K-center, the carbon-oxygen-vacancy complex COVV, causes a peak in the DLTS spectrum at a temperature of about 195 K and can be found after irradiation with electrons, protons, or helium ions. Annealing starts at temperatures between 350 and 400°C; the defect is completely annealed out at a temperature of 450°C.[5]

Table III summarizes the K-center parameters.[42] All parameters were completely determined by DLTS measurements. Although the energy level of this type of defect is relatively close to the middle of the bandgap, the contribution to recombination processes is rather small due to the low capture rates.

Defect concentration dependence on irradiation parameters.— The dependence of the K-center density on the irradiation dose is comparable to that of the OV center, as shown in Fig. 3 and 4 for electron- and helium-irradiated samples.

Effects of temporarily charged K centers.— Charged K centers influence the electrical behavior of devices because they temporarily increase the effective doping concentration in n-type silicon, thus reducing the breakdown voltage of the power device. The reduction of the breakdown voltage may cause the appearance of dynamic IMPATT (impact ionization avalanche transit-time) oscillations in diodes during the turn-off period, as illustrated in Fig. 7 for an electron-irradiated FWD.[46]

During the turn-off process, the stored carriers are extracted from the diode, and the voltage across the device increases. Under forward-bias conditions, the K center is positively charged. When the diode is turned off sufficiently fast, the defects remain positively charged for a certain time due to the relatively low electron-capture rate. The positively charged K centers increase the effective doping concentration. This reduces the breakdown voltage at the p-n junction so that avalanche multiplication sets in at diode voltages far below the static breakdown voltage. The generated electron-hole pairs are separated in the high-field zone, and the electrons moving toward the cathode reduce the positive space charge in the high-field zone. Thus, avalanche generation stops. Because the generated electrons are extracted from the high-field zone, the positive space charge can increase again, and the process just described recurs until the donorlike K centers are discharged. The frequency of this oscillation is governed by the carrier saturation velocity and the width of the low-doped region, and is typically between 200 and 1000 MHz. Dynamic IMPATT oscillations have been observed in both electron- and helium-irradiated devices.[47] Because such oscillations cause strong interfering signals, they must be avoided in high-power applications.[48]

Leakage current and compensation effects caused by divacancies and multivacancies.— Center properties.— The DLTS spectrum measured in the n^--base of a 5.4 MeV helium-irradiated FWD that was annealed at 350°C is shown in Fig. 8. In addition to the signals at $E(90\ \mathrm{K})$ and $H(195\ \mathrm{K})$, which can be attributed to the OV center and the K center, two further peaks at $E(230\ \mathrm{K})$ and $E(130\ \mathrm{K})$ are discernable. The energy levels of these peaks are 0.425 and 0.244 eV, respectively. They are usually attributed to the single negative $V_2^{(0/-)}$, and double negative, $V_2^{(-/2-)}$, charge state of the divacancy. Because divacancies anneal out at temperatures of about 300°C,[5,28] we agree (in accord with the suggestions in Ref. 49) that the two peaks are induced by the singly and doubly charged states of the V_2O defect. Another possible origin of the $E(230\ \mathrm{K})$ peak is given in Ref. 50, which suggests that it arises from a V_4 or V_5 complex.

Table IV lists the properties of $E(230\ \mathrm{K})$ after annealing at a temperature of 350°C. Energy level, entropy factor, and the electron capture rate were determined by DLTS measurements. Data for the hole-capture rate c_p could not be measured directly in our samples. Therefore, c_p was approximated based on the data published in Ref. 27 with respect to a higher ratio of c_p/c_n as suggested in Ref. 51.

While the OV complex determines essentially the electrical properties of power devices under high-injection conditions, the V_2 center is important under low-injection conditions and has a strong influence on the generation lifetime. The reason for this is that the energy level of $E(230\ \mathrm{K})$ is close to the middle of the bandgap. Although the capture rates are relatively large, indicating an effective recombination center, the influence of this defect on high-injection lifetime remains usually low because most of the defects are already annealed out at temperatures exceeding 300°C.

Defect concentration in dependence of irradiation parameters.— Figure 9 shows the density of the vacancy-related defects in dependence of the fluence for different electron energies after annealing at a temperature of $T > 330°\mathrm{C}$. Again the dependence of the defect concentration on irradiation dose is approximately linear.

Influence of annealing temperature and irradiation fluence on leakage current.— The influence of the annealing temperature and the irradiation fluence on the leakage current is illustrated in Fig. 10, where the leakage current I_R of two electron-irradiated 5-kV power diodes with a diameter of about 120 mm is depicted as a function of the annealing temperature.

The two diodes were irradiated with an electron dose of 0.2 and 1.2 kGy and an electron energy of 10 MeV. After irradiation, the diodes were first annealed for 2 h at 150°C in an inert atmosphere

Table IV. Preliminary properties of $E(230\ \mathrm{K})$ for annealing at $T > 330°\mathrm{C}$.[27,43,51]

Energy (eV)	Capture rates ($\mathrm{cm^3/s}$)		Entropy factor	
	Electrons	Holes	Electrons	Holes
$E_C - 0.43$	$3.41 \times 10^{-8}\sqrt{\frac{T}{300\ \mathrm{K}}}\exp\left(\frac{22.13 \times 10^{-3}\ \mathrm{eV\ K}}{k_B T}\right)$	$2.55 \times 10^{-5} T^{-0.84}\frac{1}{\mathrm{K}}$	0.38	2.63

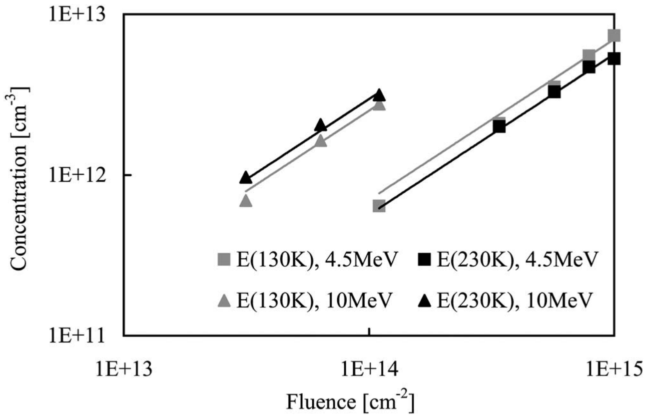

Figure 9. Concentration of the $E(130\text{ K})$ and $E(230\text{ K})$ with respect to the electron irradiation dose and irradiation energy for an annealing temperature $>330°\text{C}$.

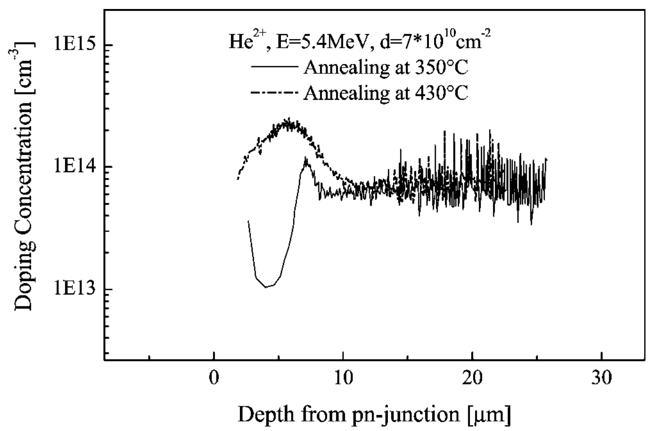

Figure 11. Doping concentration measured in the n$^-$ layer of a p$^+$-n$^-$-n$^+$ diode after helium irradiation and subsequent annealing [capacitance-voltage (*C-V*) measurement].

and the electrical parameters were measured. Then, annealing at the next higher temperature and electrical characterization were performed, and so on. The higher electron dose causes a higher concentration of divacancies and, consequently, a higher leakage current. The decreasing leakage current for both doses at annealing temperatures $T \geqslant 270°\text{C}$ indicates that the divacancies start to anneal out.

Compensation effects due to E(230 K).— Under usual annealing conditions ($T > 300°\text{C}$), the density of $E(230\text{ K})$ declines drastically. Consequently, the influence on high-injection carrier lifetime τ_{HL} is rather low even in spite of the large capture rates but remains significant for the carrier lifetime in space-charge regions τ_{SC} as well as for the low-injection lifetime τ_{LL}.

The appearance of the center $E(230\text{ K})$ influences the properties of power devices not only by modifying the charge-carrier lifetime but also due to compensation effects. This is illustrated in Fig. 11, where the doping profile inside the low-doped n-base of a helium-irradiated FWD with p$^+$-n$^-$-n$^+$ structure is shown. Without irradiation and annealing, the doping profile inside the low-doped region is homogeneous. After helium irradiation and annealing at a temperature of 350°C, the effective doping level is decreased due to the charged acceptor states of $E(230\text{ K})$. In a comparable p-type silicon diode with p$^+$-p$^-$-n$^+$ structure, $E(230\text{ K})$ is not charged because the Fermi energy level is below the energy level of the trap. Therefore, no change in the effective doping occurs (Fig. 12). Annealing at a higher temperature of $T = 430°\text{C}$ results in donor formation in the helium-irradiated area. Consequently, the effective doping increases in n-type silicon (Fig. 11), while it decreases in p-type silicon (Fig. 12).

The influence of the acceptor states on the current-voltage characteristic $I(V)$ is illustrated (Fig. 13) by a heavily helium-irradiated p$^+$-n$^-$-n$^+$ diode ($11.6\text{ MeV}, 2.1 \times 10^{12}\text{ cm}^{-2}$). The generated number of acceptor states $E(230\text{ K})$ is sufficiently large to effect a clear compensation of the background doping in the stopping range of the helium ions of approximately 70 µm. In Fig. 14, the forward $I(V)$ characteristics of this diode are shown for different temperatures. The measurements were performed using a Tektronix curve tracer model 371A by applying voltage ramps with a length of about 200 µs. Due to the generated recombination centers, not only is the on-state voltage drop across the device for a certain current increased, but the usually monotonically increasing $I(V)$ characteristic may even change to a characteristic with negative differential resistance (NDR) at low operating temperatures.

We consider a mechanism based on injection-dependent charge-carrier lifetimes to be the most probable reason for the formation of the NDR region. Such a mechanism is well-known from Au-doped silicon p$^+$-n$^-$-n$^+$ diodes.[52] Gold acts as an acceptor-like recombination center. Its hole-capture rate c_p is much larger than the electron capture rate c_n. Under low-injection conditions, the injected holes recombine immediately near the p$^+$-n$^-$ junction so that the total current is mainly carried by electrons injected from the cathode and

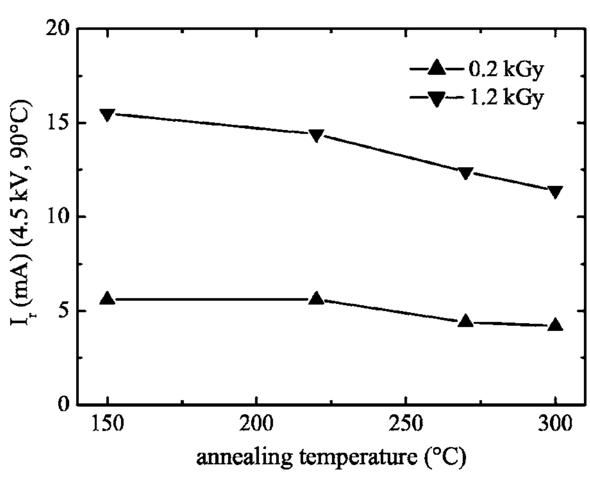

Figure 10. Leakage current dependence on annealing temperature of two electron-irradiated 5-kV power diodes.

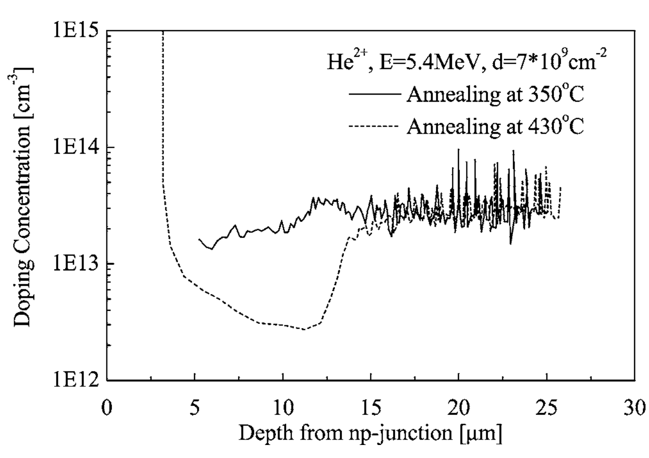

Figure 12. Doping concentration measured in the p$^-$-layer of a p$^+$-p$^-$-n$^+$ diode after helium irradiation and subsequent annealing (*C-V* measurement).

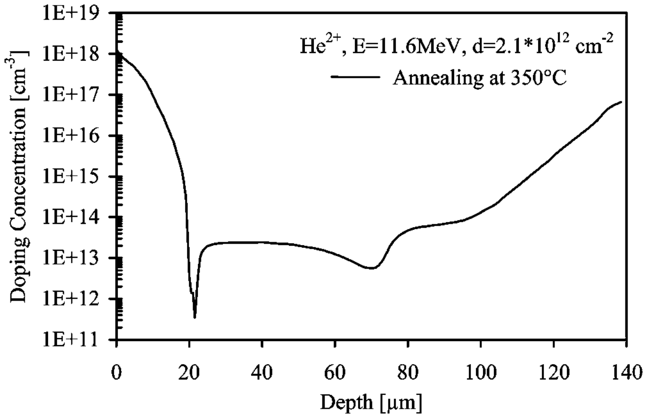

Figure 13. Change in the doping concentration of a p$^+$-n$^-$-n$^+$ diode after helium irradiation (E = 11.6 MeV, $d = 2.1 \times 10^{12}$ cm^{-2}) and subsequent annealing at 350°C [spreading resistance profile (SRP) measurement].

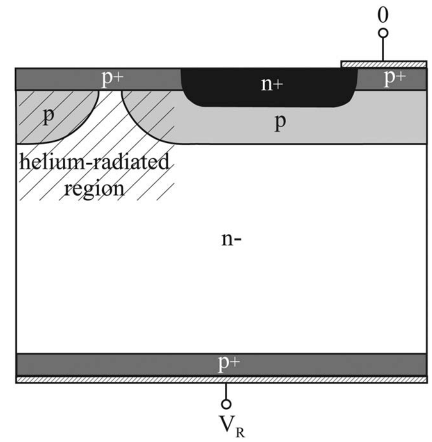

Figure 15. Circular test structure with a p-n$^-$-p structure in the center (left) and a parallel-connected thyristor (right).

most of the recombination centers in the n$^-$-layer are occupied by electrons. These occupied trap centers form a recombination barrier for holes injected from the p$^+$ layer. With increasing current, more and more holes are trapped by the recombination center. This leads to a reduction of the hole barrier so that the current can increase at a lower diode voltage, resulting in the appearance of an NDR region in the $I(V)$ characteristic.

Device simulations for our helium-irradiated p$^+$-n$^-$-n$^+$ diodes (Fig. 14) show that the observed temperature dependence of the $I(V)$ characteristic can be reproduced with the capture parameters of the $E(230\text{ K})$ defect level listed in Table IV. The appearance of the NDR region at low operating temperatures is due to the temperature dependence of c_p/c_n, which increases monotonically with decreasing temperature. That means that, for sufficiently low temperatures, the acceptor-like $E(230\text{ K})$ defect acts as a hole barrier for low currents similar to the acceptor-like Au center.

Application example using compensation effects.— Compensation effects can be exploited for the adjustment of the blocking voltage of p-n$^-$ junctions.[13] Figure 15 shows a circular test structure that consists of a p-n$^-$-p structure and a parallel-connected thyristor.[13] The central p-region is surrounded by a p-ring which acts as a field ring and is part of the vertical n$^+$-p-n$^-$-p$^+$ thyristor. The p$^+$-layer connecting the p-n$^-$-p structure and the concentric p-base of the thyristor prevents the space-charge region from reaching the surface. The device is designed to ensure that the breakdown of the upper junction of this structure occurs in the center of the concentric structure. The thickness of the n$^-$-substrate is chosen sufficiently large to ensure that the maximum electro-field strength at the p-n$^-$ junction meets the avalanche ionization criterion before the field reaches the anode p-layer. Thus the avalanche breakdown limits the maximum blocking voltage of the p-n$^-$-p structure. The thyristor connected in parallel serves to protect this structure from damage due to breakdown. This is achieved by using the avalanche current to trigger the thyristor. The typical avalanche breakdown voltage of the investigated structures is about 5 kV at room temperature. The test structures were irradiated with 24-MeV helium ions, which have a maximum penetration depth of about 300 μm. The irradiated area comprises not only the junction area but also a part of the concentric p-ring as indicated in Fig. 15. The local irradiation was performed by irradiating the sample through an aluminum mask with a pinhole; the samples were annealed for 4 h at about 220°C. In Fig. 16, the increase of the breakdown voltage after helium irradiation and annealing is shown as a function of the irradiation dose. Clearly, the breakdown voltage increases monotonically with the irradiation dose by several hundred volts, demonstrating that an adjustment of the breakdown voltage is possible even after the fabrication of a device is completed.

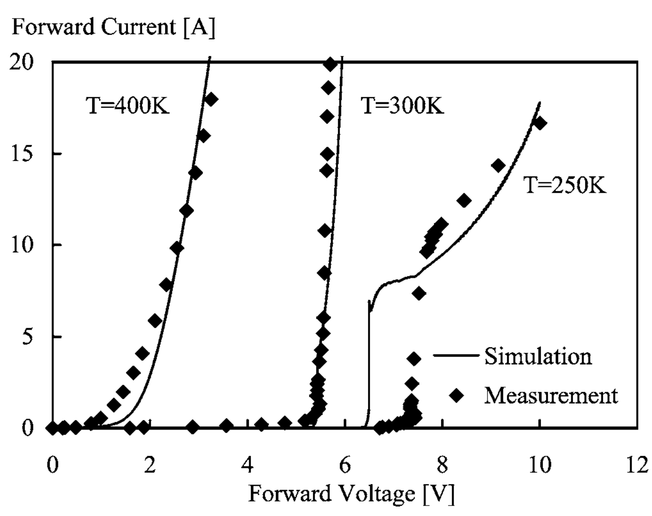

Figure 14. Measured $I(V)$ characteristics of a p$^+$-n$^-$-n$^+$ diode (A = 0.1 cm^2) after He irradiation (E = 11.6 MeV, $d = 2.1 \times 10^{12}$ cm^{-2}) and annealing at 350°C.

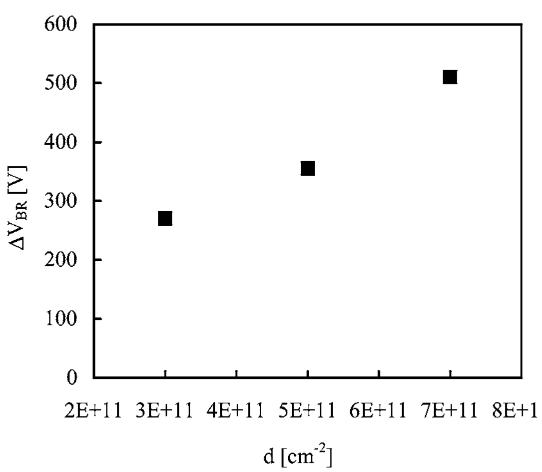

Figure 16. Increase of forward breakdown voltage ΔV_{BR} of a 5-kV p-n$^-$-p test structure after 24 MeV helium irradiation with respect to the irradiation dose d (measurement temperature 300°C).[13]

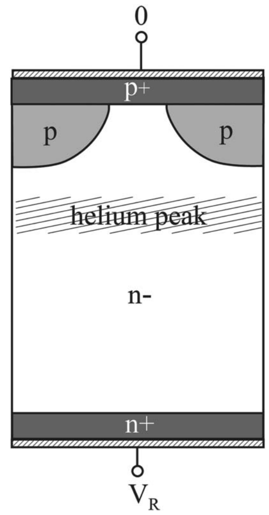

Figure 17. Simplified structure for device simulation.

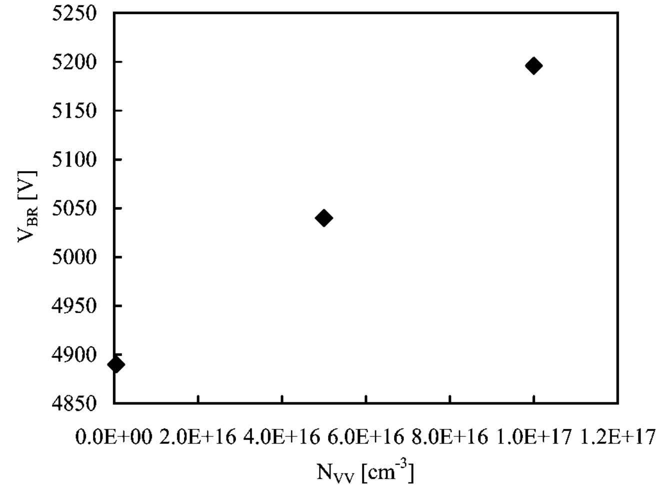

Figure 19. Breakdown voltage of the simulation structure as a function of the peak concentration N_{VV} of the divacancy distribution (cf. Fig. 20).

According to the applied annealing conditions, the acceptor-like divacancy still exists and may contribute to compensation effects. Anyway, the recombination centers are completely within the SCR region. The number of ionized acceptor-like centers is approximately

$$N_T^- = \frac{N_T}{\dfrac{c_n}{c_p}\exp\left(-\dfrac{2(E_T - E_I)}{k_B T}\right)} \qquad [11]$$

With an electron-to-hole capture rate ratio c_n/c_p of approximately 0.38 and assuming a peak density of approximately 1×10^{15} cm^{-3} for $E(230\text{ K})$, the number of ionized acceptor-like centers is

$$N_T^- \approx 1.6 \times 10^{-5} N_T \approx 1.6 \times 10^{10}\text{cm}^{-3} \qquad [12]$$

Consequently, the number of ionized centers $E(230\text{ K})$ is not sufficient to explain the increase of the blocking voltage. According to Ref. 53, the formation of divacancy clusters is possible for irradiation at high doses. Due to the high divacancy concentration (approximately 10^{20} cm^{-3}) inside the clusters, charge transfer between energy levels of neighbored divacancies is possible. This may result in an increase in the stationary negatively charged divacancy concentration inside the space-charge region by up to three orders of magnitude compared with the occupation of nonclustered divacancies.

A simplified proof of this idea was done by device simulation using TeSCA.[54] In this device simulator, the full trap dynamic is taken into account in the Poisson equation and in the charge-carrier balance equations, which is fundamental for an appropriate simulation of such devices.[42,55] However, because the device simulator TeSCA does not provide models that describe the interaction of different deep energy levels, the number of divacancies $E(230\text{ K})$ was increased by several orders of magnitude. To keep the carrier lifetimes constant, the capture rates were decreased in an appropriate way, which is possible because the number of charged acceptor states in Eq. 12 only depends on the ratio of electron- and hole-capture rates c_n/c_p. Figure 17 shows the simplified simulation structure. Figure 18 shows the simulated reverse $I_R(V_R)$ characteristics, and Fig. 19 illustrates the increase of the breakdown voltage with the number of $E(230\text{ K})$. The density of charged centers $E(230\text{ K})$ along the vertical axis is given in Fig. 20. The simulation results confirm that an increased number of stationary negatively charged divacancies, effected by clustering and simultaneous interaction of the different divacancy levels, might be responsible for increasing the avalanche breakdown voltage. Apart from the compensation effect, the reduction of the mean free path by lattice defects may cause a decrease in the avalanche generation rate, and, consequently, an

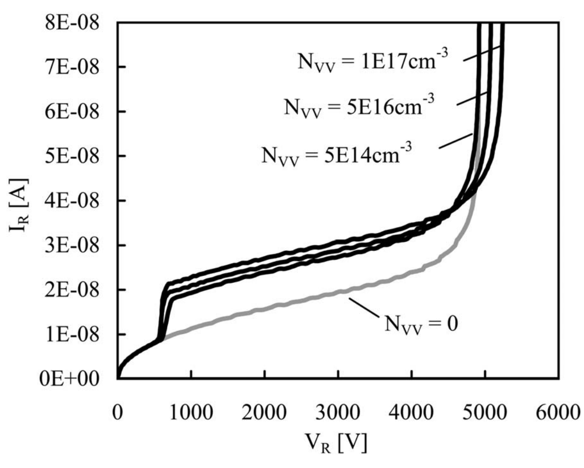

Figure 18. Simulated reverse characteristics $I_R(V_R)$ showing the influence of charged divacancies in the SCR.

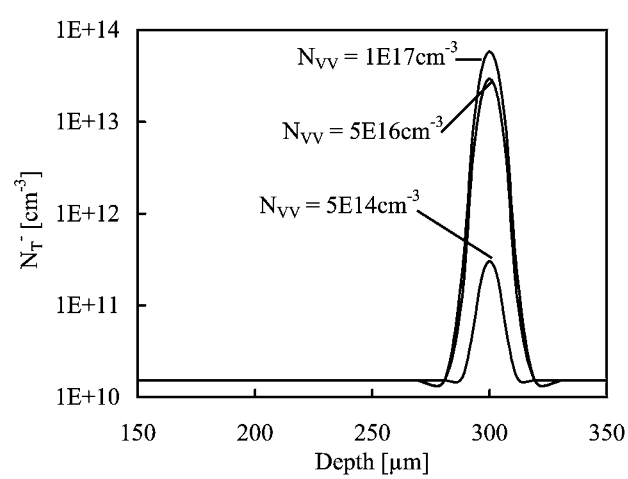

Figure 20. Density of charged divacancy states at breakdown voltage.

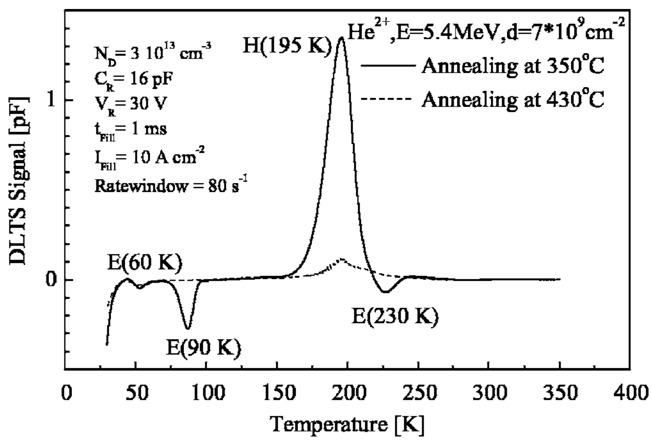

Figure 21. Minority DLTS spectra measured in the p^--layer of a p^+-p^--n^+ diode after helium irradiation and subsequent annealing.

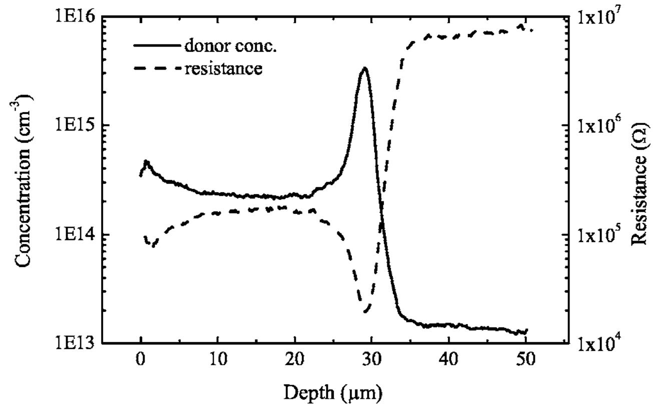

Figure 22. SR profile and resulting donor profile of a proton-irradiated (1.5 MeV, 10^{15} cm^{-2}) n-type silicon sample annealed at 500°C for 30 min; the sample was preoxidized before irradiation.[59]

increase in the breakdown voltage. Mobility measurements at silicon samples irradiated with a high dose of electrons or neutrons reveal that the mobility may decrease by more than a factor of 2.[56] We obtained similar results by investigating the influence of proton irradiation on mobility. Thus, for a quantitative comparison of the experimentally observed increase in the breakdown voltage, both compensation and mobility effects have to be taken into account.

n-type doping effects caused by thermal double donors and hydrogen-related donors.— Properties of thermal double donors.— As already shown, the annealing of helium-radiated samples at a higher temperature of 430°C results in donor formation in the helium-irradiated area. Figure 11 clearly indicates an increase in the effective doping in n-type silicon, while identical annealing results in a decrease of effective doping in p-type silicon (Fig. 12).

This donor formation in the He-irradiated area is probably caused by formation of thermal double donors (TDDs). This kind of donor formation is well-known from Cz-grown silicon with high oxygen concentration and temperature annealing, preferably between 350 and 500°C. TDDs consist of a core, [110] chains of ⟨001⟩ silicon interstitials, surrounded by different shells containing oxygen. In our samples, a relatively high oxygen concentration exists due to the preparation conditions of the diodes. The fact that donor formation is mainly observed in an area close to the penetration depth of the helium ions suggests that irradiation-induced defects are necessary to form the core for TDD formation.

Similar TDD formation has also been observed in electron-irradiated GTO thyristors fabricated from n-type FZ-grown silicon. The breakdown voltage of these GTO thyristors is limited by the punch-through effect, and reaches a maximum value after annealing at $T \approx 450°C$. From this result, it can be concluded that the thermal donor concentration in the n-base of the GTO thyristor has a maximum at this annealing temperature, which is consistent with the well-known TDD formation behavior in Cz-grown silicon. DLTS measurements (Fig. 21) show that most of the defects vanish after annealing at 430°C. In particular, the $E(230\text{ K})$ and $E(130\text{ K})$ signals are below the detection limit, indicating the disappearance of the vacancy-related defects.

Properties of hydrogen-induced donors.— Several hydrogen-related donor families formed in silicon at annealing temperatures between 250 and 500°C were identified in the past (see, e.g., Ref. 57-60). In FZ-grown silicon damaged by neutron irradiation and subsequently subjected to a hydrogen plasma treatment, hydrogen-related donors with ionization energies between 31.8 and 52.5 meV were found after temperature treatments between 250 and 400°C.[60] These donors are only formed in the presence of hydrogen if irradiation-induced damage in silicon is sufficiently high. Both conditions are also fulfilled after proton irradiation, which, in conjunction with a subsequent annealing step at temperatures between 300 and 500°C, provides an easy technique to create deep and buried n-doped layers.

A typical SR profile of a proton-implanted n-type FZ silicon sample after a 500°C annealing stage is shown in Fig. 22.[61] The minimum of the SR profile coincides with the penetration depth of the implanted 1.5-MeV protons, indicating an increased donor concentration in this region. Assuming that the whole measured sample area is of n-type conductivity, the electrically activated donor concentration profile has been calculated from the SR profile. Neither irradiation-induced effects on the charge-carrier mobility nor possible charge-carrier trapping due to irradiation-induced defects was taken into account in the calculation. The peak concentration calculated under these assumptions is about 3.3×10^{15} cm^{-3} and the integrated H-induced donor concentration is about 1.5×10^{12} cm^{-2}. Because of the high mobility of hydrogen at low temperatures, donor formation is not only effective in the heavily damaged area close to the maximum penetration depth of the implanted ions, but, to a certain extent, in the defect tail resulting in a corresponding donor tail between the peak area and the sample surface.

Application of hydrogen-related donors.— Such hydrogen-induced donor formation can be used to decrease the breakdown voltage of p-n junctions. As an example, Fig. 23 shows the breakdown voltage of two p-n^- structures with different initial breakdown voltages as a function of the annealing temperature. The two test structures have the same structure as the He-irradiated structures shown in Fig. 15, but the n^--layer is thicker and has a higher resistivity so that the

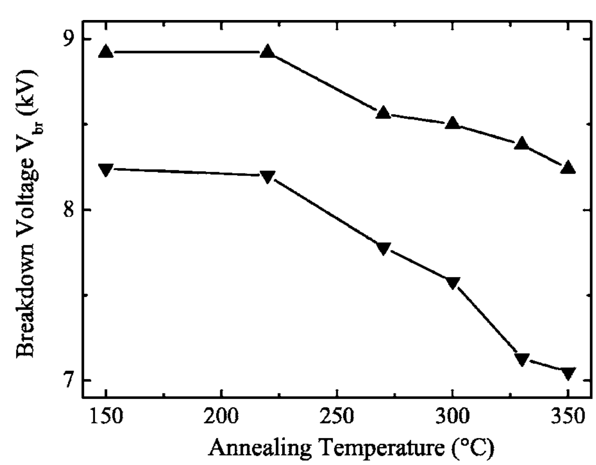

Figure 23. Breakdown voltage of two p-n^- diodes after proton irradiation (3.5 MeV, 1.2×10^{12} cm^{-2}) as a function of the annealing temperature.

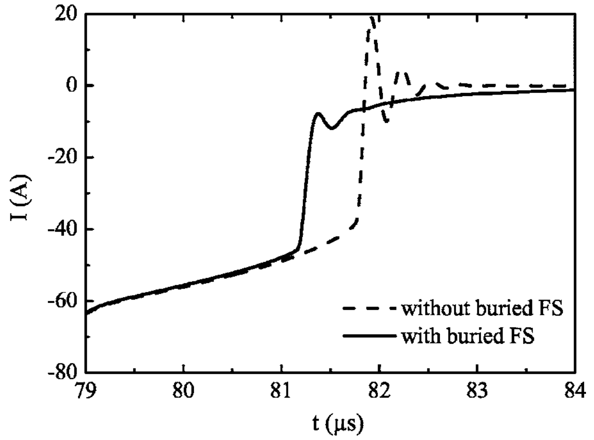

Figure 24. Simulated time series of the current for two diodes during the reverse recovery period. In the simulation, only the peak area of a typical hydrogen-induced concentration profile (cf. Fig. 22) was taken into account and approximated by a Gaussian function.[60]

initial breakdown voltages exceed 8 kV. As in the previous experiment, masked irradiation via a pinhole was performed with proton doses of 1.2×10^{12} cm^{-2} and energies of 3.5 MeV. The diodes were subsequently annealed at the specified temperatures, starting at 150°C, in each case for 2 h. As expected, a distinctive reduction of the breakdown voltage is observed for annealing temperatures higher than 220°C, indicating the formation of hydrogen-related donors.

Another example of the application of hydrogen-induced doping is the implementation of a buried field-stop layer by proton irradiation.[62,63] If the doping profile of the buried field-stop layer is optimized by properly adjusting the proton energy and flux, the electrical performance of power devices can be improved significantly. This has been shown in numerical investigations of the reverse recovery behavior of two diodes with and without an optimized field-stop layer. The diodes were turned off at a specified current turn-off rate by applying a high reverse voltage via an inductance. The time series of the diode currents are shown close to the end of the reverse recovery phase in Fig. 24. The diode without a buried field-stop layer shows a strong current decrease, accompanied by a current overshoot and large oscillations; the diode with a buried field-stop layer is free from overshoot and shows only a relatively weak and much less significant current oscillation.

Conclusion

Properties of irradiation-induced defects, which are important for tailoring the characteristics of power devices, have been reviewed. Among them are the temperature dependence of capture cross sections, the dependence of the defect density on the primary particle flux, and the annealing behavior of the defects. Several examples have been used to show how the charge states of donor-like and acceptor-like defects can modify dynamic and static characteristics of power devices. Delayed recharging of donor-like K centers, for example, may induce current oscillations during the turn-off period of diodes. Furthermore, there is experimental evidence that acceptor-like defects such as divacancy or V_2O clusters can be used to increase the static breakdown voltage of p-n^- diodes. Hydrogen-induced donor formation results in reduction of the breakdown voltage. Thus, the breakdown voltage of power devices can be tailored applying only a relatively low temperatures (<400°C) even after final device preparation.

Acknowledgments

The authors thank T. Luse, R. Schuh, G. Ahle (Infineon, Warstein), R. Bommersbach (Infineon, Munich), S. Becker, R. Herzer (Semikron, Nürnberg), and A. Möller (Fresenius, Dresden) for experimental support and helpful discussions.

References

1. F. Robb, I. Wau, and S. Ju, in *Proceedings ISPSD*, p. 251, Weimar (1997).
2. T. Nakagawa, K. Satoh, M. Yamamoto, K. Hirasawa, and K. Ohta, in *Proceedings ISPSD*, p. 175, Yokohama (1995).
3. J. Lutz, in *Proceedings EPE*, p. 1502, Trondheim (1997).
4. N. Kaminski, N. Galster, S. Linder, C. Ng, and R. Francis, in *Proceedings EPE*, Lausanne (1999).
5. W. Wondrak, Ph.D. Thesis, University of Frankfurt/M., Frankfurt/M. (1985).
6. P. Voss, German Pat. DE2817160 (1989).
7. H. Iwamoto, H. Haruguchi, Y. Tomomatsu, J. F. Donlon, and E. R. Motto, in *Proceedings IAS*, p. 692, Phoenix (1999).
8. M. Rüb, M. Bär, F.-J. Niedernostheide, M. Schmitt, H.-J. Schulze, and A. Willmeroth, in *Proceedings ISPSD'04*, p. 181, Kitakyushu (2004).
9. M. Schmitt, H.-J. Schulze, A. Schlögl, M. Vossebürger, A. Willmeroth, G. Deboy, and G. Wachutka, in *Proceedings ISPSD*, p. 229, Santa Fe (2002).
10. M. Takei, T. Naito, and K. Ueno, in *Proceedings ISPSD*, p. 156, Cambridge (2003).
11. R. Siemieniec, R. Herzer, M. Netzel, and J. Lutz, in *Proceedings MIEL*, p. 167, Nis (2004).
12. H.-J. Schulze and H. Mitlehner, in *Proceedings EPE-MADEP*, p. 393, Florence (1991).
13. F.-J. Niedernostheide, M. Schmitt, H.-J. Schulze, U. Kellner-Werdehausen, A. Frohnmeyer, and G. Wachutka, *J. Electrochem. Soc.*, **150**, G15 (2003).
14. W. Shockley and W. T. Read, *Phys. Rev.*, **87**, 835 (1952).
15. D. V. Lang, *J. Appl. Phys.*, **45**, 3023 (1974).
16. S. R. Lederhandler and L. J. Giacoletto, *Proc. IRE*, **1955**, 477 (1955).
17. R. G. Mazur and D. H. Dickey, *J. Electrochem. Soc.*, **113**, 255 (1966).
18. S. C. Jain and R. Muralidharan, *Solid-State Electron.*, **24**, 1147 (1981).
19. R. J. Basset, W. Fulop, and C. A. Hogarth, *Int. J. Electron.*, **35**, 177 (1973).
20. M. A. Green, *Solid-State Electron.*, **26**, 1117 (1983).
21. V. Grivickas, *Solid State Commun.*, **108**, 561 (1998).
22. S. Gall, Ph.D. Thesis, TU Berlin (1997).
23. JOL-R60—Gütegeschalteter diodengepumpter Festkörperlaser, Spezifikation, JENOPTIK Geschäftsbereich Lasertechnik, Jena.
24. L. C. Kimerling, H. M. Angelis, and J. Diebold, *Solid State Commun.*, **16**, 171 (1975).
25. Y. H. Lee, L. J. Cheng, and J. D. Gerson, *Solid State Commun.*, **21**, 109 (1977).
26. S. K. Bains and P. C. Branbury, *J. Phys. C*, **18**, L109 (1985).
27. H. Bleichner, P. Jonsson, N. Keskitalo, and E. Nordlander, *J. Appl. Phys.*, **79**, 9142 (1996).
28. S. D. Brotherton and P. Bradley, *J. Appl. Phys.*, **53**, 5720 (1982).
29. P. G. Fuochi, E. Gombia, R. Mosca, F. Fasce, M. Icardi, M. Portesine, and P. Rossetto, in *Proceedings EPE-MADEP*, p. 80, Firenze (1991).
30. C. A. Londos, *Phys. Status Solidi A* **113**, 503 (1989).
31. C. A. Londos and P. C. Branbury, *J. Phys. C*, **20**, 645 (1987).
32. B. G. Svenson and M. Willander, *J. Appl. Phys.*, **62**, 2758 (1987).
33. G. Ferenci, C. A. Londos, T. Pavelka, and M. Somogyi, *J. Appl. Phys.*, **63**, 183 (1988).
34. A. Hallén, N. Keskatilo, F. Masszi, and V. Nagl, *J. Appl. Phys.*, **79**, 3906 (1996).
35. P. Hazdra and J. Vobecký, *Solid-State Electron.*, **37**, 127 (1994).
36. M. W. Hüppi, Ph.D.Thesis, ETH Zürich, Zürich (1989).
37. K. Irmscher, Ph.D. Thesis, Humboldt-Universität, Berlin (1985).
38. N. Keskitalo, Ph.D. Thesis, Uppsala University, Uppsala (1997).
39. W. Südkamp, Ph.D. Thesis, TU Berlin, Berlin (1994).
40. J. R. Troxell, *Solid-State Electron.*, **26**, 539 (1983).
41. J. Vobecký, P. Hazdra, and J. Homola, *IEEE Trans. Electron Devices*, **43**, 2283 (1996).
42. R. Siemieniec, W. Südkamp, and J. Lutz, *Solid-State Electron.*, **46**, 891 (2002).
43. R. Siemieniec, W. Südkamp, and J. Lutz, in *Proceedings ICCDCS*, Aruba (2002).
44. H.-J. Schulze, A. Frohnmeyer, F.-J. Niedernostheide, F. Hille, P. Tütto, T. Pavelka, and G. Wachutka, *J. Electrochem. Soc.*, **148**, G655 (2001).
45. R. Siemieniec, W. Südkamp, J. Lutz, and M. Netzel, in *Proceedings IETA*, Cairo (2001).
46. J. Lutz, W. Südkamp, and W. Gerlach, *Solid-State Electron.*, **42**, 931 (1998).
47. R. Siemieniec, J. Lutz, and R. Herzer, *IEE Proc.-G: Circuits, Devices Syst.*, **151**, 219 (2004).
48. R. Siemieniec, M. Netzel, J. Lutz, and P. Mourick, in *Proceedings EPE*, Toulouse (2003).
49. E. V. Monakhov, B. S. Avset, A. Hallen, and B. G. Svensson, *Phys. Rev. B*, **65**, 233207 (2002).
50. J. Guldberg, *Appl. Phys. Lett.*, **31**, 578 (1977).
51. P. Hazdra, J. Rubeš, and J. Vobecký, *Nucl. Instrum. Methods Phys. Res. B*, **159**, 207 (1999).
52. I. Dudeck and R. Kassing, *J. Appl. Phys.*, **48**, 4786 (1977).
53. K. Gill, G. Hall, and B. MacEvoy, *J. Appl. Phys.*, **82**, 126 (1997).
54. H. Gajewski, B. Heinemann, and H. Langmach, *TeSCA-Handbuch*, Weierstrass-Institute for Applied Analysis and Stochastics, Berlin (1991).
55. G. K. Wertheim, *Phys. Rev.*, **100**, 1086 (1958).
56. V. F. Stas', I. V. Antonova, E. P. Neustroev, V. P. Popov, and L. S. Smirnov,

Semiconductors, **34**, 155 (2000).
57. R. C. Newman, M. J. Ashwin, R. E. Pritchard, and J. H. Tucker, *Phys. Status Solidi B*, **210**, 519 (1998).
58. V. P. Markevich, T. Mchedlidze, M. Suezawa, and L. I. Murin, *Phys. Status Solidi B*, **210**, 545 (1998).
59. J. Coutinho, R. Jones, P. R. Briddon, S. Öberg, L. I. Murin, V. P. Markevich, and J. L. Lindström, *Phys. Rev. B*, **65**, 014109 (2001).
60. J. Hartung and J. Weber, *Phys. Rev. B*, **48**, 14161 (1993).
61. H.-J. Schulze, F.-J. Niedernostheide, M. Schmitt, U. Kellner-Werdehausen, and G. Wachutka, in *High Purity Silicon VII*, C. L. Claeys, M. Watanabe, P. Rai-Choudhury, and P. Stallhofer, Eds., PV 2002-20, p. 320, The Electrochemical Society Proceedings Series, Pennington, NJ (2002).
62. F.-J. Niedernostheide, H.-J. Schulze, U. Kellner-Werdehausen, R. Barthelmess, J. Przybilla, R. Keller, H. Schoof, and D. Pikorz, in *Proceedings ISPSD'03*, p. 122, Cambridge (2003).
63. F.-J. Niedernostheide, H.-J. Schulze, U. Kellner-Werdehausen, and C. Schneider, in *Proceedings EPE*, Dresden (2005).